

RESEARCH

Open Access



# Influence of plastic shape on interim fragmentation of compostable materials during composting

Patrizia Pfohl<sup>1,2</sup>, Markus Rueckel<sup>1</sup>, Lars Meyer<sup>1</sup>, Glauco Battagliarin<sup>1</sup>, Andreas Künkel<sup>1</sup>, Thorsten Hüffer<sup>2</sup>, Michael Zumstein<sup>2</sup>, Thilo Hofmann<sup>2</sup> and Wendel Wohlleben<sup>1\*</sup>

## Abstract

Common experience with rotting wooden buildings demonstrates that fragmentation is a necessary natural process during biodegradation. In analogy, the loss of structural integrity of biodegradable plastics during biodegradation produces interim microplastic fragments. It is currently not known which parameters govern fragmentation kinetics: chemical structure, physical shape, and composite layers, or composting conditions may all be relevant. Here we investigated the influence of physical shape on the fragmentation of a polyester blend during laboratory tests simulating industrial composting. Methods previously validated on micronized granules as model shape were applied to shapes that better represent consumer products, such as micronized thin films and shredded plastic-coated paper cups. The peak interim number of detected fragments, which are between 3 and 2000  $\mu\text{m}$ , ranked highest for micronized films, lower for micronized plastic granules, and even lower for coated paper cups. The layered structure of polyester on cellulose may thus have stabilized the biodegrading polyester compound against fragmentation. For thin films, fragment counts dissipated with halftime of 2.5 days, and less than 10<sup>-8</sup>% of the initially added polyester mass was detected in fragments between 3 and 25  $\mu\text{m}$  at the last sampling time point. The physical shape and multilayer structure of the polymer-containing product were found to be decisive for fragmentation kinetics, indicating that tests on micronized polymer granules might not be representative of the release mechanism of fragments from consumer products containing plastic coatings.

**Keywords** Plastic biodegradation, Compostable plastics, Food packaging, Microplastics, Shapes, Fragmentation kinetics

## Introduction

Depending on the application and the intended end of life of (biodegradable) plastic products, mechanical, chemical, or organic recycling could be the right approach to reach circularity and to prevent plastic pollution [1–6].

For example, certified compostable organic waste bags enable a circular use of nutrients through efficient collection of organic waste for the production of organic fertilizers [7]. Another example is fiber-based compostable food packaging such as plastic-coated cups or food trays. The global sales of compostable foodservice packaging were predicted to reach USD 19.9 billion in 2022 and USD 28.8 billion by 2029, with Asia–Pacific as the region with the fastest growth [8]. The Bio-Based and Biodegradable Industries Association (BBIA) estimated that compostable plastics could substitute around 5–8% of current plastic packaging [9], whereof up to 20% of

\*Correspondence:

Wendel Wohlleben  
wendel.wohlleben@basf.com

<sup>1</sup> BASF SE, Carl-Bosch-Str. 38, 67056 Ludwigshafen, Germany

<sup>2</sup> Department of Environmental Geosciences, Centre for Microbiology and Environmental Systems Science, University of Vienna, Josef-Holaubek-Platz 2, 1090 Vienna, Austria



© The Author(s) 2024. **Open Access** This article is licensed under a Creative Commons Attribution 4.0 International License, which permits use, sharing, adaptation, distribution and reproduction in any medium or format, as long as you give appropriate credit to the original author(s) and the source, provide a link to the Creative Commons licence, and indicate if changes were made. The images or other third party material in this article are included in the article's Creative Commons licence, unless indicated otherwise in a credit line to the material. If material is not included in the article's Creative Commons licence and your intended use is not permitted by statutory regulation or exceeds the permitted use, you will need to obtain permission directly from the copyright holder. To view a copy of this licence, visit <http://creativecommons.org/licenses/by/4.0/>.

flexible packaging could be substituted, which is the fastest growing plastic-packaging category [10].

Micro- and nanoplastic fragments are expected to be formed as an interim phase before the complete metabolization of biodegradable plastic items [3, 11–18]. Some studies reported fragmentation of biodegradable plastics during biodegradation in different habitats [19–21]. However, a systematic assessment of fragmentation mechanisms and biodegradation in compost or other habitats are still missing. An assessment with commercially relevant materials is required to guide the further optimization of safer-by-design materials. Parameters controlling biodegradation are understood on a molecular level [22], but the physical fragmentation pathways might depend on the composting conditions, the polymer type, and the shape of the plastic. Material is expected to degrade faster with a more favourable surface-to-volume ratio (e.g., two-dimensional thin films vs. spherical items) [23], but little is known about the impact of shapes on the interim fragmentation [24, 25].

While previous studies addressed the final conversion of the polymer compound into biomass and CO<sub>2</sub> [18, 26], the present study focuses on the interim fragment particles during composting. We assessed the fragmentation kinetics during laboratory composting experiments of a compostable polymer compound in three shapes with increasing relevance for the product application: micronized granules (scenario A) [18], thin films (scenario B), and commercially available plastic-coated paper cups (scenario C). The methods used within this study were previously validated on model micronized granules (scenario A) and the results obtained were replotted in the present study for comparison to the new scenarios B and C [18]. Oxidation- and density-based particle extraction [27, 28], Raman microscopy ( $\mu$ -Raman) [29, 30] and fluorescence microscopy [31, 32] were employed to track the fate of the fragments. Through these steps, form, size distribution, and the chemical identity of interim fragments were determined during the composting process. The overall goal of the present study was to assess the influence of different product shapes on the fragmentation of certified compostable plastic and to quantify the interim fragmentation kinetics in each case.

## Materials

For the experiments, the certified industrially compostable ecovio<sup>®</sup> PS 1606 was used, a compound of polylactic acid (PLA) with an aromatic-aliphatic polyester [18]. In addition, a prelabelled version containing the fluorescence dye Lumogen F Yellow 083 (0.1% in weight) was used [18]. Films of ecovio<sup>®</sup> PS 1606 were produced with a thickness of 25  $\mu$ m at BASF. Certified industrially compostable paper cups with a single side coating of ecovio<sup>®</sup>

PS1606 (25  $\mu$ m) were provided by BASF (11.82 g/cup, side walls with 460  $\mu$ m thickness and specific weight 356 g/m<sup>2</sup>). The polymeric films (scenario B) were cryomilled using a Retsch ZM 200 ultra-centrifugal mill and liquid nitrogen. Films were milled with a sieving unit with a cut-off of 2 mm (flat “2D shaped” micronized films). The isolated fractions with size below the cut-off were collected and dried in a vacuum oven at 36 °C for 48 h. The ecovio<sup>®</sup> PS1606 coated paper cups were cut to separate bottom and side pieces. To ensure homogeneity, only the side walls were taken without the folded top rim and without the bottom. Shredding was performed with a common office shredder producing flat (“2D shaped”) pieces in the size of 12 mm  $\times$  2 mm. Shredding was preferred to cryo-milling to avoid possible delamination of the polymer compound film from the paper layer. For polymer compound characterization, laser diffraction (method description published in [33]), gel permeation chromatography (GPC) and differential scanning calorimetry (DSC) measurements were carried out for scenarios A, B, C and are described in the Supporting Information (Table S1).

## Methods

### Composting: disintegration test under industrial composting conditions of cryo-milled (prelabelled and non-labelled) ecovio<sup>®</sup> films and shredded paper cups

The compost experiments for scenarios B and C were performed according to the conditions described in standard ISO 20200:2015 “*Plastics – Determination of the degree of disintegration of plastic materials under simulated composting conditions in a laboratory-scale test*”. For the experiments, plastic boxes with 5.5 L volume (32.7 cm  $\times$  22.7 cm  $\times$  11.1 cm) were used. To allow air exchange during the experiment, two holes were drilled at a 6.5 cm height of the side of dimension 22.7 cm  $\times$  11.1 cm. Different compost batches were used in each scenario, which is why all compost blanks have been extracted and analysed for possible contaminations and for comparison to the timepoints investigated in each scenario. Two different experimental campaigns were run for the tested materials: 1) For the cryo-milled and prelabelled films a total of 7 boxes were used: 1 box containing compost without any plastic test material, 6 boxes with the compost and cryo-milled films of prelabelled ecovio<sup>®</sup>; 2) For the non-labelled materials a total of 17 boxes was used: 1 box containing compost without any plastic material, 8 boxes with the compost and shredded paper cups and 8 boxes with the cryo-milled films of ecovio<sup>®</sup> PS1606. A 12-14-week-old compost (OWS, Belgium) was sieved to remove pieces bigger than 10 mm and 1200 g were mixed with 300 g fresh vegetables (celery, carrots, and fennel) and 30 g of test substance

(ecovio® PS1606 films or shredded paper cups). For the pre-labelled ecovio® films (campaign 1) the dry content was 64.2% and pH 7.8. For the non-labelled ecovio® films and the shredded paper cups (campaign 2) the dry content was 66.7% and pH 7.8. The coated paper samples were wetted with water before starting the experiment to avoid drying of the compost. After closing the boxes, the samples were incubated at 58 °C for 45 days. The content of the boxes was mixed at day 7, 14, 21 and 28 and water content adjusted. Samples of the compost containing pre-labelled ecovio® films were taken at day 0, 10, 20 and 45. For the non-labelled films and the shredded paper cups two replicates were stopped after 5, 10, 20 and 45 days. At the end of the experiment the boxes were opened and dried at 58 °C until upon drying no further weight loss was observed. The compost extracts with pre-labelled films were analyzed by fluorescence microscopy. The compost extracts with non-labelled films and paper coatings were analyzed by  $\mu$ -Raman microscopy.

The experimental conditions for scenario A were described in detail elsewhere [18]. To improve readability an overview on experimental conditions for each scenario investigated is provided in Fig. 1.

#### Extraction – density-based fragment method

The extraction builds on the process developed for the analysis of polyester-polyurethane microplastics in compost [34], and was optimised for the specific polyester compound elsewhere [18, 33]. In short, multiple steps (homogenization, oxidation, sieving, density separation) are needed to remove the compost components. For each of those steps, specific control tests for polymer and particle stability, recovery and matrix removal efficiency in the overall process were done for validation. In this study 55 wt.-% ( $\rho = 1.5 \text{ g/cm}^3$ ) calcium chloride ( $\text{CaCl}_2$ , VWR Chemicals, technical) salt solution was used instead of the previously used 50 wt.-% ( $1.4 \text{ g/cm}^3$ ) zinc chloride ( $\text{ZnCl}_2$ , Bernd Kraft) salt solution for density separation,

and the sedimentation time was reduced from 60 to 24 h. The initial film size was 2 mm (scenario B) and  $2 \times 12 \text{ mm}$  (scenario C), which is too large for a reliable analysis by the microscopy techniques, since these might cover the smaller secondary fragments. This is why the original film pieces were removed in our 1 mm sieving step and the microscopy techniques analyzed the secondary fragments  $< 1 \text{ mm}$  only. Details on the method and controls can be found in our previous publication [18] and in the SI. After sediment removal the supernatant was analysed by Raman and fluorescence microscopy as described before [18]. Details are given in the SI.

## Results

### Protocol optimization and controls for isolation of biodegradable microplastic fragments

To enable the monitoring of biodegradable polymer fragmentation and degradation during composting, an efficient and valid microplastic extraction protocol is needed. The microplastic extraction protocol used for this study and its controls were reported before [18], but adjustments and additional controls were done for further improvement. Specifically, the salt solution and sedimentation time were optimized, and the need for oxidation was re-evaluated. The systematic investigations of Scenario A, B and C had used density separation by  $\text{ZnCl}_2$  (A) and by  $\text{CaCl}_2$  (B, C), respectively. This change was motivated by the lower toxicity and lower acidity of  $\text{CaCl}_2$  [35], and cross-checks were performed: specifically, extraction efficiency on scenario A was compared with density separation either by  $\text{ZnCl}_2$  or  $\text{CaCl}_2$ , each adjusted to the same density (tested on 70 days and 187 days samples: Figure S1). In addition, the sedimentation time was reduced from 60 h (with  $\text{ZnCl}_2$ ) to 24 h (with  $\text{CaCl}_2$ ), which imposes a lower limit of quantitative extraction at  $10 \mu\text{m}$  particle size (Stokes–Einstein law) but seemed acceptable due to the detection limits imposed anyway by the

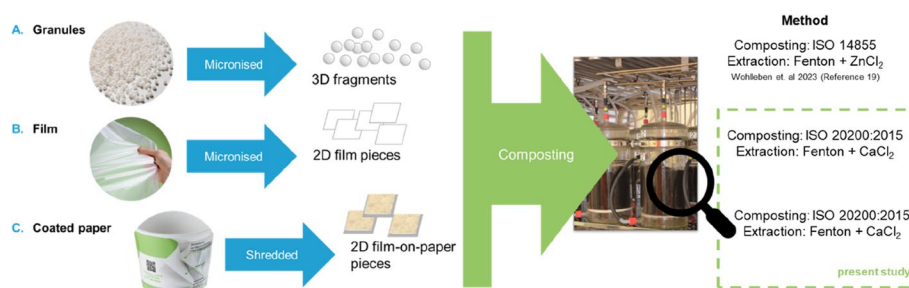


**Fig. 1** Scenarios tested on three form factors (A: fragments [18], B: films, C: coated paper) of the same polyester-PLA polymer compound under industrial composting conditions. The thinnest initial dimension is  $330 \mu\text{m}$  diameter for the micronized fragments,  $25 \mu\text{m}$  thickness for the micronized film and for the polymer compound coating layer on paper ( $460 \mu\text{m}$  overall thickness)

spatial resolution of the microscopes. The cross-checks showed on the compost with 70 days incubation of the micronized granules (scenario A), that the total numbers found were 19,110 (with  $\text{CaCl}_2$ ) and 16,680 (with  $\text{ZnCl}_2$ ), which is a 15% difference, but the normalized particle size distribution showed a bias of the Ca-based extraction to smaller, and of the Zn-based extraction to larger particles (Figure S1a). Larger polymer particle numbers with Ca-based extraction indicate that this method is more representative, especially for the size fraction below 25  $\mu\text{m}$ . The same comparison was applied to the last time point of 187 days. The total particle numbers found were 1589 (with  $\text{CaCl}_2$ ) and 130 (with  $\text{ZnCl}_2$ ), which is a 12-fold difference, but the normalized particle size distribution was practically indistinguishable (Figure S1b). Especially the degradation (not accumulation) of the fragments below 25  $\mu\text{m}$  that we had earlier reported with  $\text{ZnCl}_2$  separation [18] was clearly confirmed also with  $\text{CaCl}_2$  separation. As additional check, also scenario B was investigated at the last time point of 45 days with both  $\text{CaCl}_2$  separation and  $\text{ZnCl}_2$  separation. We found a 16-fold lower fragment number with  $\text{ZnCl}_2$ , but a consistent share of the size bin of 25 to 75  $\mu\text{m}$ , which was 50% (with  $\text{CaCl}_2$ ) and 58% (with  $\text{ZnCl}_2$ ). Both density separation options

confirmed that in scenario B there were no particle counts between 3  $\mu\text{m}$  and 25  $\mu\text{m}$ , in contrast to scenario A.

It has been argued that oxidation is required to ensure proper identification of microplastics, notably by removing biofilm from fragments [29, 36]. In the present study the combination of ultrasonication and oxidation was additionally beneficial to separate the polymer coating from the paper (scenario C), and thus to make all fragments of the polymer coating visible in the microscopy analysis. Using Nile Red staining and fluorescence microscopy (as done for scenario A), it was possible to also analyse extracts without oxidation, since the particle size distribution was the same and the total number of fragments per gram compost (26,083/g without oxidation, 26,383/g with oxidation) was indistinguishable (Figure S2). We note that nonetheless *all* results in the present contribution were obtained *with* oxidation, to suppress background counts from fresh compost such as the one used in scenarios B and C.

Representative images of the morphology of fragments highlighted the roughened three-dimensional shape of the micronized polymer compound (Fig. 2a) against the flat “2D shaped” platelet-shape of the micronized films with sharp contours (Fig. 2c). During industrial

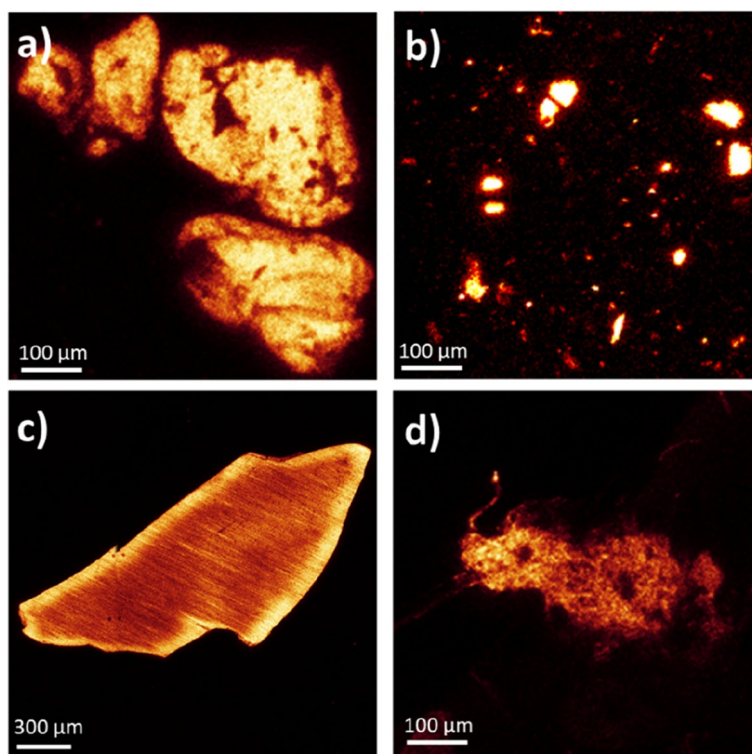


**Fig. 2** Morphology of Nile-red stained fragments observed by fluorescence microscopy: **a, b**) micronized plastic granules extracted from compost at **a**) 0 days; **b**) 70 days. **c, d**) micronized plastic films extracted from compost at **c**) 0 days; **d**) 20 days

composting, the smooth surface of the films developed locally thinner regions and roughened contours (Fig. 2d). Using  $\mu$ -Raman, additionally to the size also the identity of each particle was deduced by the “ParticleScout” software (WITec Wissenschaftliche Instrumente und Technologie GmbH, Ulm) by fitting the spectrum against a preconfigured library, which we had amended by polymer compound spectra (Fig. 3). Due to the lower spatial resolution of the  $\mu$ -Raman, the contours were less crisp than by fluorescence, and agglomerated fragments may have been counted as one larger fragment (Fig. 3). However,  $\mu$ -Raman is still higher-resolving than the alternative of FTIR microscopy [27, 37, 38].

### Scenarios tested by the experimental design

The main aim of this study was to investigate the hypothesis that fragmentation of biodegradable polymers during composting depends on the product shape. For this purpose, three scenarios (A: cryo-milled granules, B: cryo-milled films, C: shredded coated paper) were compared. Due to the micronized size of the initial polymer compound loading in the compost, the standardized mass of ecovio<sup>®</sup> in dry compost of 12 wt.-% (scenario A) and 3 wt.-% (scenario B) corresponds to several thousand initial (scenario A) and interim (scenario B) fragment counts per gram of dry compost. We chose these micronized fragments to allow a statistical analysis and to obtain solid data, which would not be possible with macroscopic items, because the resulting fragments would not be homogeneously distributed in the compost. The three different scenarios increase in realism from model fragments to the actual commercial item:

- A) Irregular micronized plastic granules with roughly isotropic thickness in all 3 dimensions (Fig. 2a), which were in the focus of our previous publication [18]. Percentiles of the size distribution were  $D_{10}=119\ \mu\text{m}$ ,  $D_{50}=331\ \mu\text{m}$ ,  $D_{90}=673\ \mu\text{m}$  (160% polydispersity by laser diffraction). This size is an order of magnitude higher than the thickness used for the ecovio<sup>®</sup> PS1606 grade in paper coating application (ranging between 10–30  $\mu\text{m}$ ) and above the certified thickness for industrial composting applications. This scenario is relevant for mechanistic comparison only. The results were obtained in our previous study [18] and are summarized for comparison to scenarios B and C: Fragments of 25 to 75  $\mu\text{m}$  size represented the most pronounced peak of interim fragmentation, which was reached already after 1 week of composting (Fig. 1 in [18]). Larger sizes peaked earlier while the smaller size population peaked later.
- B) Micronized plastic films with 25  $\mu\text{m}$  thickness, simulating a more realistic scenario. The test material consists of anisotropic film fragments of irregular circumference in 2 dimensions but homogeneous thickness (Fig. 2c). Percentiles of the size distribution were  $D_{10}=50\ \mu\text{m}$ ,  $D_{50}=175\ \mu\text{m}$ ,  $D_{90}=990\ \mu\text{m}$  (530% polydispersity by laser diffraction).
- C) Commercially available paper cups represented an actual product used by the end consumer. After shredding in a document shredder, the shape was anisotropic (25  $\mu\text{m}$  coating of polymer compound on paper) and consisted of a single-side coated paper of the size of 12 mm  $\times$  2 mm with less than 20% polydis-

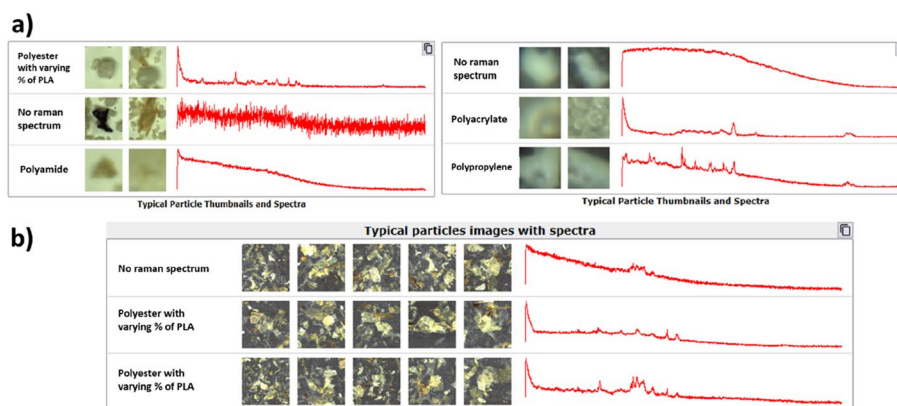


**Fig. 3**  $\mu$ -Raman thumbnails of fragments and their spectra after industrial composting. **a)** micronized ecovio<sup>®</sup> PS1606 granules after 7 days (scenario A); **b)** micronized ecovio<sup>®</sup> PS1606 films after 10 days (scenario B). A Raman spectrum in the interval 3600 to 50  $\text{cm}^{-1}$  was acquired for each particle on the filter for up to  $N=30,000$  total particles, resulting in the statistical representation of particle size and identity in the Supplementary Information (compare to data in our previous publication [18] and the detailed Tables S4 and S5). Each thumbnail has a field of view adapted to the respective particle

persity, and initially no presence of small fragments in the detection range below 1000 μm.

GPC and DSC measurements of all three shapes were conducted to understand if fragmentation might also depend on the production pathway (Table S1). Since all shapes were made from the same polyester compound, the chemical and thermal properties were comparable. In general, the range between 30.000 and 130.000 g/mol is typical for thermoplastic polymers [39]. The number average molar mass ( $M_n$ ) was quite similar between the different shapes, while the weight average molar mass ( $M_w$ ) was slightly higher for the coated paper than for the other shapes, but we can't exclude the presence of any additives extracted from the paper itself. In all three shapes investigated, the melt enthalpy representing the crystallinity was low [40] and the melt temperature was in a consistent range around 166 °C.

**Scenario A: fragmentation kinetics of micronized plastic granules show particle shrinkage and fragmentation**

In our previous publication we monitored the CO<sub>2</sub> evolution over time for scenario A, reaching >90% biomineralization after 187 days of industrial composting [18]. Note that the long composting times are due to the initial thickness exceeding by an order of magnitude the thickness range certified for industrial composting applications of ecovio® PS1606. The results obtained in the previous study [18] were replotted for a comparison to the other shapes investigated in the present study (Fig. 4). Numerical values of Raman microscopy measurements for scenario A have been reported before [18], numerical values for fluorescence microscopy are reported in Table S2.

For Fig. 4a, the sum of all particles with spectra attributable to the aromatic-aliphatic polyester ecovio® PS1606 is plotted, integrating the previously published detailed findings in different size classes [18]. In short, the fragment count was reduced by nearly three orders of magnitude from 8207 to 3 ± 3 particles per gram of compost, while the total LDPE counts changed by an insignificant extent of 7% with no signs of chemical degradation during industrial composting (Fig. 4a) [18]. The associated size distribution of the aromatic-aliphatic polyester fragments shifted to smaller fragments (Fig. 4c), but fragmentation led to an interim increase of total particle counts after 7 days of composting (Fig. 4b); however, those previously formed fragments reduced to 3 ± 3 particles per gram of compost, which was indistinguishable from the blank count of 5 ± 5 particles per gram of compost after 187 days [18].

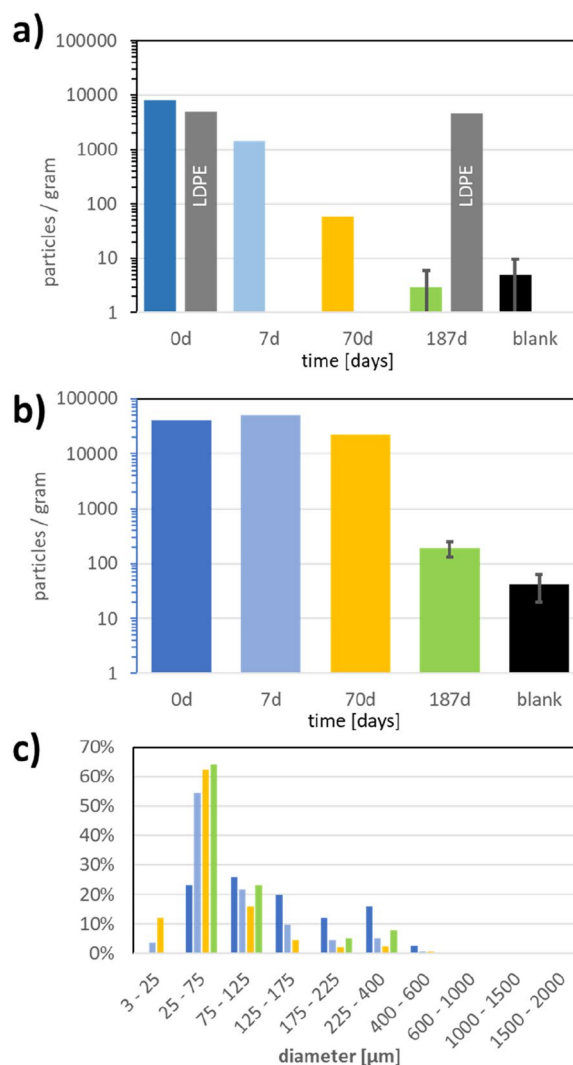


**Fig. 4** ecovio® PS1606 fragments per gram of compost after worst-case scenario A spiking by micronized ecovio® PS1606, then particle extraction (using ZnCl<sub>2</sub>) and analytics [18]. Results compared to LDPE and compost blank. **a)** total number of ecovio® fragments by μ-Raman microscopy; **b)** total number of polymer fragments by fluorescence microscopy; **c)** particle size distribution (area-equivalent diameter) for each timepoint by fluorescence microscopy

**Scenario B: fragmentation kinetics of cryo-milled plastic film show peninsula structure formation and fragmentation**

Quantitative disintegration experiments under laboratory industrial conditions were performed to investigate fragmentation of the cryo-milled film samples. The initial polymer compound mass and the number of fragments per gram of compost, due to the large lateral dimensions of the 25 μm thin films, was lower in scenario B compared to A. The findings in scenario B showed a six-fold

increase of fragment numbers (Fig. 5a, Table S3). Fragmentation was confirmed by the very quick increase of fragment numbers (Fig. 5a), which could only originate from the fragmentation of film pieces, not by erosion and volume loss only. The degradation of the largest films above 400 μm (compare Fig. 2c) was well-documented in the size distribution by fluorescence microscopy (Fig. 5b) and was confirmed by the μ-Raman size distribution (Figure S3b, Table S4). Only the fragments above 100 μm were counted using μ-Raman, and no fragments were found after 45 days (Figure S3a, Table S4), which is in agreement with the size distribution by fluorescence microscopy (Fig. 5b). The relative share of the size fraction from 25 to 125 μm increased until the last sampling time point and is responsible for the slight increase of fragment count between 20 and 45 days, while fragments above 175 μm almost entirely disappeared during this time interval (Fig. 5b). Fragments between 3 and 25 μm were not observed, not even intermittently at a single

time point. This is another marked difference between scenarios A and B.

The half-time of particle count was 2.5 days (micronized films, scenario B), to be compared to 20 days (micronized granules, scenario A). A detailed description of the half-time calculations is provided in the SI. The differences in half-time are consistent with the 25 μm thin flat geometry of the films, offering more surface area than the 330 μm micronized particles. Surface-driven enzymatic degradation also induces that smaller fragment sizes have shorter lifetimes [23, 41], as explained on the detailed fragmentation kinetics earlier [18]. Even intermittently, the maximum share of fragments between 3 and 25 μm observed amounted to 12% by number (observed by fluorescence microscopy on ecovio® PS1606 scenario A at 50% CO<sub>2</sub>), corresponding to 0.0012% by mass (Fig. 6a, b), and even less for the thin films (scenario B, Fig. 6c). By the last sampling, this mass fraction dropped below 10<sup>-10</sup> of initial polymer compound mass

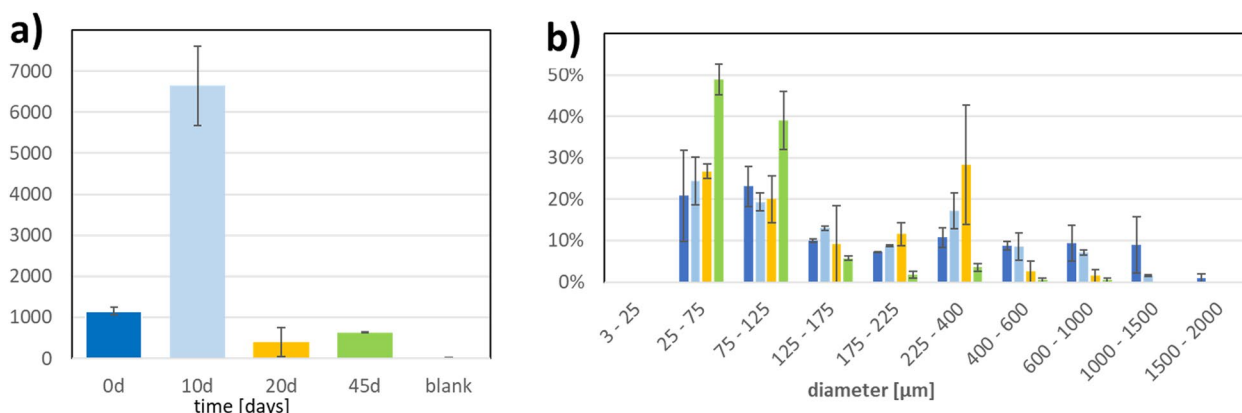


**Fig. 5** Scenario B: Polymer compound fragments per gram of compost after spiking by micronized ecovio® PS1606 films, then particle extraction and fluorescence detection. Results compared to compost blank. **a)** total numbers; **b)** particle size distribution for each time point

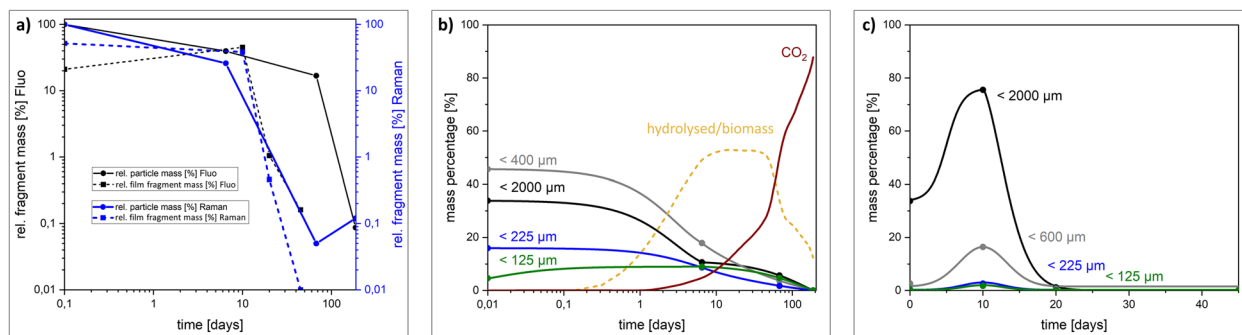


**Fig. 6** Kinetics of fragment degradation in mass metrics. **a)** relative mass of micronized granules and films compared each to initial polymer compound mass extracted, **b)** relative mass of several size fractions compared to the conversion to CO<sub>2</sub>, for the worst-case-scenario A (micronized granules) [18], **c)** relative mass of several size fractions compared to initial polymer compound mass extracted for scenario B (micronized films). Calculations are based on the measured particle size distributions and numbers from fluorescence and Raman microscopy at the specific timepoints, representing all fragments above 3 μm and below 2000 μm. The fitted curves represent a guide to the eye and are no numerical model yet

(Fig. 6a) without accumulation of small fragments. The potential correction by the more representative extraction by  $\text{CaCl}_2$  must be considered for scenario A, but in mass metrics the 12-fold higher count of the smallest fraction by  $\text{CaCl}_2$  is invisible at 187 days, because it corrects the mass of fragments at this timepoint from  $10^{-10}$  to  $10^{-9}$  of the initial polymer compound mass.

### Scenario C: fragmentation kinetics of plastic-coated paper show local thinning without fragmentation

Contrary to the other scenarios, the polymer-coated paper cups were not micronized but only shredded into relatively large pieces of 2 mm by 12 mm before mixing with compost to perform composting experiments following the same conditions used for the cryo-milled films (scenario B). This scenario reflects the realistic industrial composting of paper-based packaging, starting from macroscopic articles that potentially release microscopic fragments during the biodegradation. The shredded pieces were still easily seen at 10 days (Figure S4) but disintegrated such that they were not visually observable at 20 and 45 days (Figure S4). Motivated by the need for chemical selectivity, the fragments extracted from compost of polymer-coated paper were identified and counted primarily using  $\mu$ -Raman (Table S5). In the specific composting series, there was a slightly higher background in the blank control of 35 polymer particles per gram of compost. Their spectrum matched the biodegradable ecovio<sup>®</sup> PS1606 reference, but an identification as PBT or PET could not be excluded; occasionally they also contained  $\text{TiO}_2$ , indicating a source other than the polymer-coated paper, e.g., white pigment contained in the paper cups. Figure 7 shows the absolute values. By subtraction of the blank, the highest fragment count at 5 days composting amounted to  $28 \pm 29$  polymer compound particles per gram of compost (triplicate extraction and analysis, Fig. 7a). At 20 and 45 days, the counts gradually decreased to blank level (Fig. 7a). In most cases, the morphology of the fragments whose spectra were attributed to the ecovio<sup>®</sup> PS1606 polymer compound were flat and confirmed the origin from delamination and fragmentation of the paper coating (Fig. 7b), similarly to the morphology of the 25  $\mu\text{m}$  thin films (Fig. 2c, d), but fewer counts than for the films (Fig. 5a). Compost particles without Raman spectrum, or PET or PE microplastics, did not resemble the flat coating fragments (Fig. 7b). Due to the low statistical count, all fragments matching the reference spectrum of the compostable ecovio<sup>®</sup> PS1606 with varying % of PLA were summed up for the fragmentation kinetics (Fig. 7a) and for an aggregated size distribution (Table S5). On a selected larger fragment (Fig. 7c) we acquired multiple Raman spectra (Fig. 7d) showing that the attribution to the ecovio<sup>®</sup>

PS1606-based paper coating is unambiguous despite some variability of the spectra on several spots of the polymer compound layer, which were fitted with varying % of PLA. In our previous investigation of scenario A, the composition of the polymer compound shifted gradually to lower PLA content during the biodegradation [18]. Degradation of one polymer from a blend induces volume loss. We observed cracks in the polymer compound layer after 5 days composting using fluorescence microscopy (Fig. 7f), which were reminiscent of the local thinning of free-standing films (Fig. 2d) and were absent in the paper coating before composting (Fig. 7e). Holes or loosely connected structures, which had formed in free-standing films (Fig. 2d), were not observed in this exemplary image of biodegraded polymer-coated paper (Fig. 7f).

### Discussion

To enable a comparison between different plastic shapes in the investigated scenarios, the influence of the extraction protocol needs to be considered: The measured size distribution shifted to smaller fragments in the early phases of scenario A (Figure S1a), where the  $\text{ZnCl}_2$  extraction efficiency is known to be lower than  $\text{CaCl}_2$  extraction efficiency. Based on the cross-checks (Figure S1), the 20% increase of fragment numbers from 40,987 to 49,263 per gram of compost measured by the  $\text{ZnCl}_2$  separation (Fig. 4b) can be translated to an increase of 38%. With the  $\text{CaCl}_2$  separation, the contribution of fragmentation is confirmed by the more relevant fraction of fragments below 25  $\mu\text{m}$  (Figure S1a), which had also been observed, but to a lesser extent, with  $\text{ZnCl}_2$  separation on the size fraction below 25  $\mu\text{m}$  and between 25 and 75  $\mu\text{m}$  (Fig. 4c). The variations of the extraction protocol thus impact quantitative details of the fragment size distributions, but confirm qualitatively different pathways of the fragmentation kinetics for scenarios A and B.

The polymer compound loading used for scenarios B and C and the more active compost reflect more realistic conditions as compared to biodegradation experiments done for scenario A, but this test does not allow the tracking of evolved  $\text{CO}_2$  during the biodegradation process. Biodegradation-induced fragmentation was most markedly observed in scenario B, which is the biodegradation of a free-standing film: the shifts in the size distribution and the sharp initial increase of total particle counts could only be explained by *fragmentation*, not by *erosion* and ensuing volume loss. To a lesser extent, also scenario A confirmed biodegradation-induced fragmentation. Control measurements showed that this observation was not an artifact induced by the sonication step during extraction; in literature the use of sonication for deagglomeration is recommended [18, 27, 42–44]. We

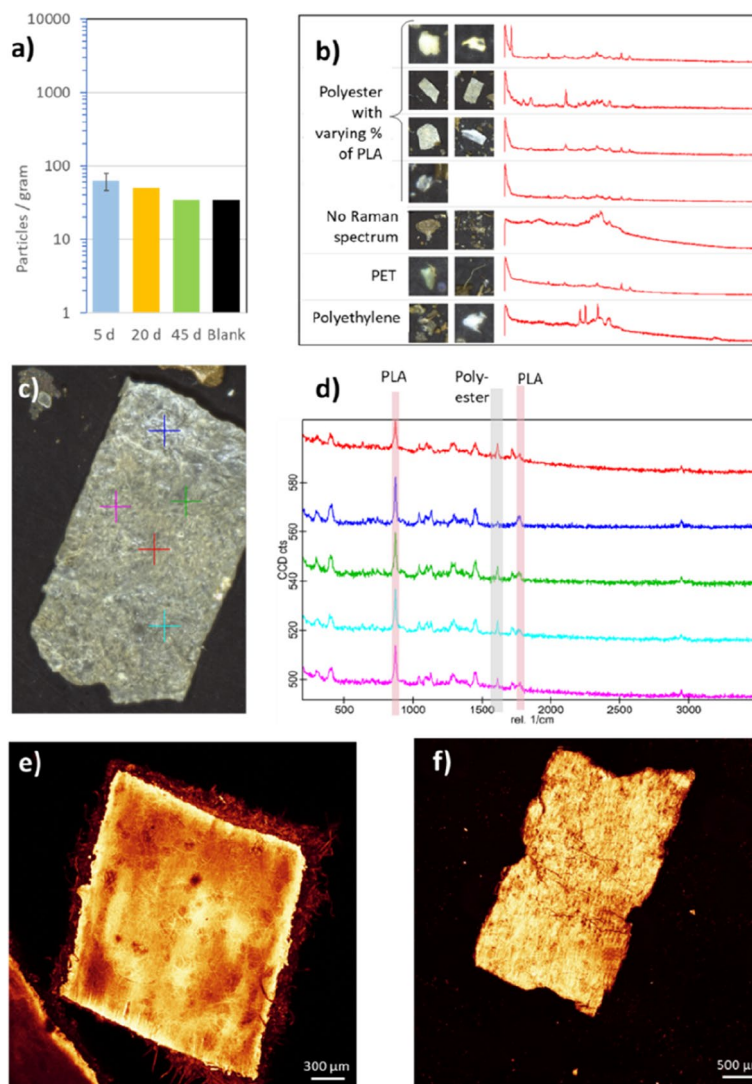


**Fig. 7** Scenario C: characterization of polymer compound fragments from composting of coated paper. **a)** A total numbers of fragments that matched the reference spectrum of the biodegradable ecovio® PS1606 with varying % of PLA; **b)** μ-Raman thumbnails of fragments and their spectra after 5 days of composting and removal of cellulose by oxidation and density separation; **c-d)** μ-Raman analysis of a representative large fragment after 5 days of composting and removal of cellulose by oxidation and density separation; **e)** higher-resolution image by fluorescence microscopy of a polymer compound coated paper before it entered the composting phase (with cellulose fibres visible underneath); **f)** representative fragment after 5 days of composting imaged by fluorescence microscopy, without oxidation or density separation

argue that the microbial colonisation and enzymatic hydrolysis on two sides of the plastic films induced local thinning that is spatially inhomogeneous on the order of 50 μm laterally (Figs. 2d and 7f), e.g. by local degradation from exudated enzymes around the fungal hyphae as imaged on the same length scale by Zumstein et al. (2018), who investigated the biodegradation of polyesters in soils. [26] Especially the formation of loosely connected “peninsula” structures is prone to fragmentation (Fig. 2d). In scenario A, the contribution of fragmentation to the particle kinetics was less obvious in μ-Raman

data, but the redistribution of particle sizes was observed by the higher resolving fluorescence microscopy (Fig. 4). The mass balance of detectable particles (Fig. 6b) and detectable CO<sub>2</sub> highlights the conversion from initially all solid polymer to a coexistence of solid polymer (i.e. particles), CO<sub>2</sub>, and a fraction of breakdown intermediates and/or biomass. The interim existence of breakdown intermediates/biomass was inferred here by subtracting %CO<sub>2</sub> and %particle from the known initial polymer compound loading (Fig. 6b), and is consistent with the previous demonstration of two fractions of the polymer

molar mass distribution at 10% CO<sub>2</sub> and at 50% CO<sub>2</sub>, namely a high molar mass fraction (identified as bound in particles) and the low molar mass (present in compost outside of particles), whereas the molar mass distribution matched the blank compost background at 90% CO<sub>2</sub> [18].

Reduction of molar mass and depolymerization drives a competition between *overall* loss of volume and *local* loss of volume, that is governed by the spatial inhomogeneity of microbial action, and by the shape of the plastic article (and, after initial fragmentation, shape of fragment). *Local* loss of volume induces a thinning to labile necks between two volumes of the fragment, but at the same time *all* volumes shrink due to surface erosion [41] and may thus disappear before that neck breaks. In scenario C, the initially incubated 2 mm x 12 mm shreds of polymer compound coating on paper were observed to disintegrate (Figure S4), but only a very low number of fragments below 2 mm could be attributed to the polymer compound coating (Fig. 7b-d) and the number of fragments was barely above the blank background (Fig. 7a). Since all test materials were made of the same polyester polymer compound, the minor differences in molecular properties (specifically a higher molar mass was measured on polymer-coated paper, almost identical melting points and even lower crystallinity of the polymer-coated paper (Table S1)) are unlikely to explain reduced fragmentation. The accessibility of the polymer chains for enzymes attacking the amorphous phases cannot be radically different under these conditions [42]. We interpret that although the polymer compound coating on paper had the same composition, same flat geometry and same thickness as the free-standing film, the additional mechanical support from the paper stabilized the plastic layer against fragmentation. The paper was removed by sample preparation (oxidation), and hence we would have detected any fragments that were only held together by the paper support. The paper substrate also halves the possibility of microbial attack to only one surface of the compostable plastic coating, but we do not suggest that this factor alone is responsible for low fragmentation. The fragments formed in scenario C (Fig. 7b, c, f) were identical in composition and shape to the intentionally micronized films spiked into the compost in scenario B (Fig. 2c), and a complete mass balance, potentially enabled by <sup>13</sup>C labelled polymer, should be targeted for a mechanistic understanding of the supported structures on paper, and the continued degradation of its fragments.

Wei et al. (2022) attributed the 10 μm fragments observed after the incubation of poly(ε-caprolactone) in an abiotic aqueous lipase buffer to the uneven hydrolysis/erosion rate across the polymer film surface. [19] In addition, normalized size distributions (Figs. 4 and 5)

highlight the continuous redistribution from larger to smaller sizes. At the final phases of degradation, total count decreased with half-times around 20 days (scenario A) to 2.5 days (scenario B).

The initial content of *polymer compound* per dry compost was in line with the ISO standards, but different between the three tested scenarios: 0.130 g/g (A), 0.030 g/g (B), 0.007 g/g (C). Polymer compound mass was used to normalize the number of fragments. For scenarios A and B the increase of the particle count between T<sub>0</sub> and the first sampling was considered, while for scenario C the maximum count above blank was considered. As a result, the number of fragments in the size range 3 to 2000 μm that were generated per gram composted polymer compound were 64.000 (scenario A), 183.000 (scenario B), and 4.000 (scenario C). The shape of specimen is thus decisive for the extent and kinetics of fragmentation [41]. In contrast to mm-sized particles of conventional plastics, such as PS, PE, PET, that were still found in organic fertilizer after biowaste fermentation or composting, fragments of biodegradable polymers undergo complete biodegradation and in our cases returned to blank level for any polymer form [14, 45].

## Conclusions

In this study, the influence of different product shapes on the fragmentation of certified compostable plastic, ecovio® PS1606, was investigated under industrial composting conditions. Disintegration of this material, independent from the shape, did not lead to the release of *persistent* microplastic fragments. Even though interim secondary fragments were formed for micronized granules and micronized films (scenarios A and B), the smallest detectable fragments (between 3 and 25 μm) did not accumulate over time and were rarely observed in any of our experiments. From CO<sub>2</sub> and GPC measurements [18] on scenario A, we additionally observed complete biodegradation which makes the hypothetical formation of nanoplastic [46, 47] fragments unlikely. Although the present observation cannot explicitly rule out their presence due to the flotation speed and microscopic detection measurement limits, we strongly believe that the microscopy techniques would have detected persistent fragments between 3 and 25 μm if they were present.

The measured half-lives of particles are around 20 days (micronized granules, scenario A) to 2.5 days (micronized films, scenario B). This is consistent with the different thickness of 330 μm (micronized granules, scenario A) against 25 μm (micronized films, scenario B), which is the realistic thickness that enters composting plants via commercial application in paper-based food packaging. In the present study, the industrial composting experiments were carried out on a laboratory scale. As a next

step, validation, and standardisation of the methodology for a big scale industrial composting facility is envisioned to enable its application to municipal facilities.

#### Abbreviations

CO <sub>2</sub>	Carbon dioxide
BBIA	Bio-Based and Biodegradable Industries Association
LDPE	Low density polyethylene
PLA	Polylactic acid

#### Supplementary Information

The online version contains supplementary material available at <https://doi.org/10.1186/s43591-024-00084-8>.

#### Supplementary Material 1.

#### Acknowledgements

We would like to thank Daniel Bahl, Florian Hornberger, Christoph Link, Christian Roth, Marion Wagner, and Lukas Leibig for excellent lab work (extractions and analysis). We are also sincerely grateful to Sarah Jessl (present address: TU Munich) and Eynat Biedermann for the conception of the seminal experiments.

#### Authors' contributions

The manuscript was written through contributions of all authors. All authors have given approval to the final version of the manuscript.

#### Funding

PP and WW were partially funded by BMBF (German Federal Ministry of Education and Research) within the InnoMat.Life project (funding no: 03XP0216X). MZ, THü, and THo were funded by the University of Vienna.

#### Availability of data and materials

All data generated or analyzed during this study are included in this published article and its supplementary information files.

#### Declarations

#### Ethics approval and consent to participate

Not applicable.

#### Consent for publication

Not applicable.

#### Competing interests

MZ, THü, THo declare no conflicts of interest. WW, MR, LM, GB, AK and PP are employees of BASF, a company producing both conventional and biodegradable plastics, including the ecovio® PS1606 investigated here.

Received: 17 October 2023 Accepted: 13 March 2024

Published online: 21 March 2024

#### References

- Kakadellis S, Rosetto G. Achieving a circular bioeconomy for plastics. *Science*. 2021;373:49–50. <https://doi.org/10.1126/science.abj3476>.
- Persson L, Carney Almroth BM, Collins CD, Cornell S, de Wit CA, Diamond ML, Fantke P, Hassellöv M, MacLeod M, Ryberg MW, Søgaard-Jørgensen P, Villarrubia-Gómez P, Wang Z, Hauschild MZ. Outside the safe operating space of the planetary boundary for novel entities. *Environ Sci Technol*. 2022;56:1510–21. <https://doi.org/10.1021/acs.est.1c04158>.
- MacLeod M, Arp HPH, Tekman MB, Jahnke A. The global threat from plastic pollution. *Science*. 2021;373:61–5.
- Bergmann M, Mützel S, Primpke S, Tekman MB, Trachsel J, Gerdt G. White and wonderful? Microplastics prevail in snow from the Alps to the Arctic. *Sci Adv*. 2019;5:eaax1157.
- European Commission Directorate General for Environment; Hilton M, Geest Jakobsen L, Hann S, Favoino E, Molteni S, Scholes R. Relevance of biodegradable and compostable consumer plastic products and packaging in a circular economy. Publications Office; 2020. <https://doi.org/10.2779/497376>.
- Eunomia. Relevance of Conventional and Biodegradable Plastics in Agriculture. Final report to the European Commission DG Environment, Contract No ENV.B1/FRA/2018/0002 Lot 1. 2021. <https://environment.ec.europa.eu/system/files/2021-09/Agricultural%20Plastics%20Final%20Report.pdf>.
- von Vacano B, Mangold H, Vandermeulen GW, Battagliarin G, Hofmann M, Bean J, Künkel A. Sustainable Design of Structural and Functional Polymers for a Circular Economy. *Angew Chem*. 2022;62:e2022108. <https://doi.org/10.1002/anie.202210823>.
- Future Market Insights. Compostable Foodservice Packaging Market By Packaging Type (Plates, Trays, Bowls, Cups, Clamshell, Cutlery, Pouches & Sachets and Others), Material (Plastic, Paper & Paperboard and Others), End Use & Region Forecast to 2022 - 2029. <https://www.futuremarketinsights.com/reports/compostable-foodservice-packaging-market>, Accessed 2021.
- Bio-based\_and\_Biodegradable\_Industries\_Association. BBIA Position Paper on Standards for Biodegradable, Compostable and Bio-based Plastics, 2019. can be accessed at <https://bbia.org.uk/reports/>.
- Ellen\_MacArthur\_Foundation. We need compostable packaging, but it's still single-use. <https://www.ellenmacarthurfoundation.org/articles/we-need-compostable-packaging-but-its-still-single-use>. Accessed 2022.
- Liao J, Chen Q. Biodegradable plastics in the air and soil environment: Low degradation rate and high microplastics formation. *J Hazard Mater*. 2021;418:126329. <https://doi.org/10.1016/j.jhazmat.2021.126329>.
- Qin M, Chen C, Song B, Shen M, Cao W, Yang H, Zeng G, Gong J. A review of biodegradable plastics to biodegradable microplastics: Another ecological threat to soil environments? *J Clean Prod*. 2021;312:127816. <https://doi.org/10.1016/j.jclepro.2021.127816>.
- Rillig MC, Lehmann A. Microplastic in terrestrial ecosystems. *Science*. 2020;368:1430. <https://doi.org/10.1126/science.abb5979>.
- Weithmann N, Möller JN, Löder MG, Piehl S, Laforsch C, Freitag R. Organic fertilizer as a vehicle for the entry of microplastic into the environment. *Sci Adv*. 2018;4:eaap8060.
- Rutgers M, Faber M, Waaijers-van der Loop SL & Quik JTK. Microplastics in soil systems, from source to path to protection goals: State of knowledge on microplastics in soil. RIVM report 2021–0224, 2022. <https://doi.org/10.21945/RIVM-2021-0224>
- Chen Y, Leng Y, Liu X, Wang J. Microplastic pollution in vegetable farmlands of suburb Wuhan, central China. *Env Pollut*. 2020;257:113449.
- Zhang GS, Liu YF. The Distribution of Microplastics in Soil Aggregate Fractions in Southwestern China. *STOTEN*. 2018;642:12–20.
- Wohlleben W, Rückel M, Meyer L, Pfohl P, Battagliarin G, Hüffer T, Zumbstein MT, Hofmann T. Fragmentation and Mineralization of a Compostable Aromatic-Aliphatic Polyester during Industrial Composting. *Environ Sci Technol Lett*. 2023;10:698–704. <https://doi.org/10.1021/acs.estlett.3c00394>.
- Wei X-F, Capezza AJ, Cui Y, Li L, Hakonen A, Liu B, Hedenqvist MS. Millions of microplastics released from a biodegradable polymer during biodegradation/enzymatic hydrolysis. *Water Res*. 2022;211:118068. <https://doi.org/10.1016/j.watres.2022.118068>.
- Weinstein JE, Dekle JL, Leads RR, Hunter RA. Degradation of bio-based and biodegradable plastics in a salt marsh habitat: another potential source of microplastics in coastal waters. *Mar Pollut Bull*. 2020;160:111518. <https://doi.org/10.1016/j.marpolbul.2020.111518>.
- Sintim HY, Bary AI, Hayes DG, English ME, Schaeffer SM, Miles CA, Zelenyuk A, Suski K, Flury M. Release of micro- and nanoparticles from biodegradable plastic during in situ composting. *Sci Total Environ*. 2019;675:686–93. <https://doi.org/10.1016/j.scitotenv.2019.04.179>.
- Witt U, Einig T, Yamamoto M, Kleeberg I, Deckwer W-D, Müller R-J. Biodegradation of aliphatic-aromatic copolyesters evaluation of the final biodegradability and ecotoxicological impact of degradation intermediates. *Chemosphere*. 2001;44:289–99.

23. Chinaglia S, Tosin M, Degli-Innocenti F. Biodegradation rate of biodegradable plastics at molecular level. *Polym Degrad Stab.* 2018;147:237–44. <https://doi.org/10.1016/j.polymdegradstab.2017.12.011>.
24. Yang H-S, Yoon J-S, Kim M-N. Dependence of biodegradability of plastics in compost on the shape of specimens. *Polym Degrad Stab.* 2005;87:131–5. <https://doi.org/10.1016/j.polymdegradstab.2004.07.016>.
25. Boyandin AN, Prudnikova SV, Karpov VA, Ivonin VN, ĐĐ NL, Nguyễn TH, Lê TMH, Filichev NL, Levin AL, Filipenko ML, Volova TG, Gitelson II. Microbial degradation of polyhydroxyalkanoates in tropical soils. *Int Biodeterior Biodegradation.* 2013;83:77–84. <https://doi.org/10.1016/j.ibiod.2013.04.014>.
26. Zumstein MT, Schintlmeister A, Nelson TF, Baumgartner R, Woebken D, Wagner M, Kohler H-PE, McNeill K, Sander M. Biodegradation of synthetic polymers in soils: Tracking carbon into CO<sub>2</sub> and microbial biomass. *Sci Adv.* 2018;4:1–8.
27. Möller JN, Löder MG, Laforsch C. Finding microplastics in soils: a review of analytical methods. *Environ Sci Technol.* 2020;54:2078–90.
28. Ruggero F, Gori R, Lubello C. Methodologies for Microplastics Recovery and Identification in Heterogeneous Solid Matrices: a review. *J Polym Environ.* 2020;28:739–48. <https://doi.org/10.1007/s10924-019-01644-3>.
29. Araujo CF, Nolasco MM, Ribeiro AMP, Ribeiro-Claro PJA. Identification of microplastics using Raman spectroscopy: Latest developments and future prospects. *Water Res.* 2018;142:426–40. <https://doi.org/10.1016/j.watres.2018.05.060>.
30. Ghosal S, Chen M, Wagner J, Wang ZM, Wall S. Molecular identification of polymers and anthropogenic particles extracted from oceanic water and fish stomach - A Raman micro-spectroscopy study. *Environ Pollut.* 2018;233:1113–24. <https://doi.org/10.1016/j.envpol.2017.10.014>.
31. Maes T, Jessop R, Wellner N, Haupt K, Mayes AG. A rapid-screening approach to detect and quantify microplastics based on fluorescent tagging with Nile Red. *Sci Rep.* 2017;7:1–10.
32. Tamminga M. Nile Red Staining as a Subsidiary Method for Microplastic Quantification: A Comparison of Three Solvents and Factors Influencing Application Reliability. *SDRP J Earth Sci Environ Stud.* 2017;2. <https://doi.org/10.15436/jeses.2.2.1>
33. Pfohl P, Roth C, Meyer L, Heinemeyer U, Gruending T, Lang C, Nestle N, Hofmann T, Wohlleben W & Jessl S. Microplastic extraction protocols can impact the polymer structure. *Microplastics and Nanoplastics.* 2021;1. <https://doi.org/10.1186/s43591-021-00009-9>
34. Pfohl P, Bahl D, Rückel M, Wagner M, Meyer L, Bolduan P, Battagliarin G, Hüffer T, Zumstein M, Hofmann T, Wohlleben W. Effect of Polymer Properties on the Biodegradation of Polyurethane Microplastics. *Environ Sci Technol.* 2022. <https://doi.org/10.1021/acs.est.2c05602>.
35. Braun, U. Statuspapier Mikroplastik-Analytik - Probennahme, Probenaufbereitung und Detektionsverfahren. *Plastik in der Umwelt.* 2020. [https://bmbf-plastik.de/sites/default/files/2020-11/Statuspapier\\_Mikroplastik%20Analytik\\_Plastik%20in%20der%20Umwelt\\_2020.pdf](https://bmbf-plastik.de/sites/default/files/2020-11/Statuspapier_Mikroplastik%20Analytik_Plastik%20in%20der%20Umwelt_2020.pdf). Accessed 2021.
36. Al-Azzawi MS, Kefer S, Weißer J, Reichel J, Schwaller C, Glas K, Knoop O, Drewes JE. Validation of sample preparation methods for microplastic analysis in wastewater matrices—reproducibility and standardization. *Water.* 2020;12:2445.
37. Hüffer T, Praetorius A, Wagner S, Von Der Kammer F, Hofmann T. Microplastic exposure assessment in aquatic environments: learning from similarities and differences to engineered nanoparticles. *Environ Sci Technol.* 2017. <https://doi.org/10.1021/acs.est.6b04054>.
38. Primpke S, Christiansen SH, Cowger W, De Frond H, Deshpande A, Fischer M, Holland EB, Meyns M, O'Donnell BA, Ossmann BE, Pittroff M, Sarau G, Scholz-Böttcher BM, Wiggin KJ. Critical Assessment of Analytical Methods for the Harmonized and Cost-Efficient Analysis of Microplastics. *Appl Spectrosc.* 2020;74:1012–47.
39. Lechner MD, Gehrke K, Nordmeier EH. *Makromolekulare Chemie.* Vol. 3. Birkhäuser Basel; 2003.
40. Hiemenz PC, Lodge TP. *Polymer Chemistry, vol. Second.* Taylor & Francis Group: Edition (CRC Press; 2007.
41. Haider TP, Völker C, Kramm J, Landfester K, Wurm FR. *Plastics of the Future? The Impact of Biodegradable Polymers on the Environment and on Society.* *Angew Chem Int Ed.* 2019;58:50–62. <https://doi.org/10.1002/anie.201805766>.
42. Pfohl P, Bahl D, Rückel M, Wagner M, Meyer L, Bolduan P, Battagliarin G, Hüffer T, Zumstein M, Hofmann T, Wohlleben W. Effect of Polymer Properties on the Biodegradation of Polyurethane Microplastics. *Environ Sci Technol.* 2022;56:16873–84. <https://doi.org/10.1021/acs.est.2c05602>.
43. Möller JN, Heisel I, Satzger A, Vizsolyi EC, Oster SDJ, Agarwal S, Laforsch C, Löder MGJ. Tackling the challenge of extracting Microplastics from soils: a protocol to purify soil samples for spectroscopic analysis. *Environ Toxicol Chem.* 2022;41:844–57. <https://doi.org/10.1002/etc.5024>.
44. Tophinke AH, Joshi A, Baier U, Hufenus R, Mitrano DM. Systematic development of extraction methods for quantitative microplastics analysis in soils using metal-doped plastics. *Environ Pollut.* 2022;311:119933. <https://doi.org/10.1016/j.envpol.2022.119933>.
45. Gui J, Sun Y, Wang J, Chen X, Zhang S, Wu D. Microplastics in composting of rural domestic waste: Abundance, characteristics, and release from the surface of macroplastics. *Environ Pollut.* 2021;274:116553.
46. Gigault J, El Hadri H, Nguyen B, Grassl B, Rowczeny L, Tufenkji N, Feng S, Wiesner M. Nanoplastics are neither microplastics nor engineered nanoparticles. *Nat Nanotechnol.* 2021. <https://doi.org/10.1038/s41565-021-00886-4>.
47. Mitrano DM, Wick P, Nowack B. Placing nanoplastics in the context of global plastic pollution. *Nat Nanotechnol.* 2021. <https://doi.org/10.1038/s41565-021-00888-2>.

### Publisher's Note

Springer Nature remains neutral with regard to jurisdictional claims in published maps and institutional affiliations.